University of Kentucky
UKnowledge

Pharmaceutical Sciences Faculty Publications | Pharmaceutical Sciences

5-17-2022

Cerium dioxide, a Jekyll and Hyde nanomaterial, can increase basal and decrease elevated inflammation and oxidative stress

Robert Yokel
University of Kentucky, ryokel@uky.edu

Marsha L. Ensor
University of Kentucky

Hemendra J. Vekaria
University of Kentucky

Patrick G. Sullivan
University of Kentucky

See next page for additional authors

Right click to open a feedback form in a new tab to let us know how this document benefits you.

Follow this and additional works at: https://uknowledge.uky.edu/ps_facpub

 Part of the Pharmacy and Pharmaceutical Sciences Commons

Cerium dioxide, a Jekyll and Hyde nanomaterial, can increase basal and decrease elevated inflammation and oxidative stress

Digital Object Identifier (DOI)
https://doi.org/10.1016/j.nano.2022.102565

Authors
Robert Yokel, Marsha L. Ensor, Hemendra J. Vekaria, Patrick G. Sullivan, David J. Feola, Arnold Stromberg, Michael T. Tseng, and Douglas A. Harrison

This article is available at UKnowledge: https://uknowledge.uky.edu/ps_facpub/206

Cerium dioxide, a Jekyll and Hyde nanomaterial, can increase basal and decrease elevated inflammation and oxidative stress

Robert A. Yokel[a*], Marsha L. Ensor[a], Hemendra J. Vekaria [b,c], Patrick G. Sullivan [b,c], David J. Feola[d], Arnold Stromberg[e], Michael T. Tseng[f†], Douglas A. Harrison[g]

[a] Pharmaceutical Sciences, University of Kentucky, Lexington, Kentucky, 40536-0596, US

[b] Spinal Cord & Brain Injury Research Center, University of Kentucky, Lexington, Kentucky, 40536-0509, US

[c] Neuroscience, University of Kentucky, Lexington, Kentucky, 40536-0509, US

[d] Pharmacy Practice and Science, University of Kentucky, Lexington, Kentucky, 40536-0596, US

[e] Statistics, University of Kentucky, Lexington, Kentucky, 40536-0082, US

[f] Anatomical Sciences & Neurobiology, University of Louisville, Louisville, Kentucky, 40202,

[†] Deceased December 17, 2019.

[g] Biology, University of Kentucky, Lexington, Kentucky, 40506-022, US

Funding: This work was supported by the National Institutes of Health [grant number R01GM109195]. The content is solely the responsibility of the authors and does not necessarily represent the official views of the National Institutes of Health.

Conflicts of interest: The authors have no conflicts of interest.

Word count, Abstract: 141

Word count, manuscript including body text and figure legends: 6090

Number of references: 60

Number of figures: 7

Number of tables: 3

* Corresponding author

Robert A. Yokel, Ph.D.

Department of Pharmaceutical Sciences

University of Kentucky Academic Medical Center

335 Todd (College of Pharmacy) Building

789 S. Limestone

Lexington, KY, 40536-0596, US

phone: 859-257-4855

fax: 859-257-7564

e-mail: ryokel@uky.edu

ORCID: 0000-0001-5188-3972

Introduction

Nanoceria (nanoscale cerium oxide, cerium dioxide, ceria, CeO_2) are metal oxide engineered nanomaterials extensively used industrially and shown to have beneficial pharmaceutical properties. They are auto-catalytically redox active, cycling between Ce^{+3} and Ce^{+4} [1]. Their surface has oxygen vacancies in its cubic fluorite structure that allow it to easily accept and donate oxygen, providing catalytic properties. Nanoceria are used as catalysts in diesel fuel, abrasives in chemical mechanical planarization in integrated circuit manufacture, as structural supports for catalysts for fuel synthesis applications, in solid oxide fuel cells, and in rechargeable batteries [2].

Nanoceria have been demonstrated to have therapeutic potential for many conditions with an inflammation/oxidative stress component including cancer, radiation damage, bacterial infection, sepsis, wounds, stroke-induced ischemia, retinal degeneration, and neurodegenerative diseases (Introduction of Yokel et al [3]). Nanoceria have shown utility as a component of sensors for biomolecular recognition (nanozymes) [4]. On the other hand, nanoceria have been demonstrated to have adverse effects, including cytotoxicity in multiple cell lines [5], genotoxicity [6], pulmonary toxicity [7, 8], hepatotoxicity [9, 10], reproductive system toxicity [11], potential neurotoxicity [12], and cardiovascular toxicity [13, 14]. In many of these studies toxicity was attributed to nanoceria-induced increased inflammation and oxidative stress. Nanoscale cerium oxide was selected by the Organisation for Economic Co-operation and Development (OECD) Working Party on Manufactured Nanomaterials as one of 13 representative manufactured nanomaterials for safety testing [15]. The above Jekyll and Hyde actions of nanoceria led to the hypothesis that, as a catalyst, nanoceria have the potential to increase inflammation from the basal state (activation of unpolarized (M0) macrophages toward the pro-inflammatory (M1) state or repolarize anti-inflammatory (M2) macrophages toward the M1 phenotype) and to decrease

inflammation from the elevated state (decrease activation of pro-inflammatory (M1) and anti-inflammatory cells (M2) macrophages).

Nanoceria have been shown to be taken up by activated U937 (human leukemic monocyte lymphoma), mouse macrophage J774A.1, and RAW 264.7 cells [16 17 18 19]; human monocyte-derived macrophages [20]; into rat red and white pulp macrophages following intravenous administration [21]; and into macrophage lysosomes following intratracheal instillation [22]. Macrophages can exist in their unpolarized (M0) state or in activated states, simplistically as classically activated, pro-inflammatory cells involved in host defense (M1) or an alternatively activated, regulatory phenotype (M2), which have some opposing actions [23]. Nanoparticles have been shown to be differentially taken up by M1 compared to M2 polarized macrophages [24 25 26 27 28, 29]. We found human monocyte-derived macrophages and RAW 264.7 cells that were converted to M1- and M2-like cells took up the same 4 nm ceria particles utilized in the present study, but the intracellular nanoceria localization and concentration differed between the phenotypes (Unpublished results submitted for publication). Nanoparticles have been shown to effect macrophage phenotype, activating them [30 31 32 33 34], changing their polarization profile [35], converting M2-like macrophages toward more M1-like cells [36 37 38 39], and repolarizing M1 macrophages toward the M2 phenotype [40 41].

Some prior work has investigated the ability of nanoceria to repolarize mononuclear phagocytes. Intratracheal nanoceria initiated a response one day later in rats suggestive of M1 polarization [42]. The response of dendritic cells to nanoceria was dominated by the TH2 cytokines IL-4, IL-5, and IL-10 [43]. Administration of intravenous nanoceria to rats that also received intraperitoneal lipopolysaccharide (LPS) attenuated release of M1 phenotype markers [19]. Incorporation of nanoceria into hydroxyapatite coatings resulted in multiple indicators suggestive of a RAW 264.7 cell switch to the M2 phenotype [44]. We are not aware of studies that

determined the effects of nanoceria on all three states, unpolarized (M0) and polarized (M1 and M2) macrophages. The following experiments were conducted to address the above hypothesis.

Methods

The materials, material sources, and nanoceria preparation and characterization are in the Supplementary Material. The methods for RAW 264.7 cell culture and polarization are in the Supplementary Material.

RAW 264.7 cell preparation for experimentation

For experiments that included nanoceria exposure, the medium was changed to a high glucose, phosphate-free Dulbecco's Modified Eagle's Medium (DMEM) plus 10% FBS during the vehicle or nanoceria exposure to avoid nanoceria-phosphate precipitation. The nanoceria vehicle was 0.11 sodium citrate, pH 7.4.

Interleukin-1β (IL-1β) and arginase assays

For the IL-1β and arginase assays the cells were scraped into 0.5 ml phosphate-buffered saline (PBS), centrifuged to pellet the cells, resuspended in 0.1% Triton-X 100-PBS with the addition of a Roche protease inhibitor cocktail tablet, vortexed, and centrifuged to remove non-lysed cells. The supernatant was collected and stored at -80 °C.

Macrophage gene expression determined by RT-qPCR

RAW 264.7 cells (passage 8 to 10) were plated in 6 well plates (Corning #3516) in 10% FBS-DMEM (plus phosphate) at a density of 4.5 x 10^5/well (sub-confluent). Eighteen h post-plating, the cells were washed with 10% FBS-DMEM (minus phosphate). The nanoceria vehicle or nanoceria was added to the cells in 10% FBS phosphate-free DMEM followed by incubation for 2.5 h in a 37 ˚C, 5% CO_2 incubator. The cells were washed once with saline

and then 10% FBS-DMEM (plus phosphate), polarized, and then incubated for 6 h in a 37 ˚C, 5% CO_2 incubator. The cells were prepared for RNA purification by washing three times with PBS, centrifugation (184 rcf for five min) to collect the cell pellets and stored at -80 ˚C until RNA purification.

RAW cell RNA was purified using Qiagen RNeasy Mini Kits, with the addition of 10 µl β-mercaptoethanol/ml in Buffer RLT. DNA digestion was conducted using Qiagen RNase-Free DNase Set. Mouse spleen RNA (endogenous reference) was also purified using the above kit and digestion set. The RNA concentration was measured using a Nano Drop 2000 (Thermo-Fisher Sci, ND-2000). RNA was stored at -80 ˚C until the cDNA was prepared.

cDNA was prepared using the iScript cDNA synthesis kit, using either 800 or 1000 ng/20 µl reaction, depending on RNA yield, following the manufacturer's cycle times and temperatures. The reaction included 80-100 ng RNA, 4 µl 5x iScript reaction mix, 1 µl iScript reverse transcriptase, and nuclease free water added to 20 µl total volume. A Bio-Rad C100 Touch Thermal Cycler was used for DNA amplification, programmed for priming (5 min at 25 °C), reverse transcription (RT) (20 min at 46 °C), and RT inactivation (1 min at 95 °C). After synthesis, the cDNA was stored at -80 °C.

The qPCR reactions were run in 96 well plates containing 50 ng cDNA, 5 µl TaqMan Fast Advanced Master Mix, 0.5 µl TaqMan Gene Expression Assay, and nuclease free water in 10 µl total volume. The plates were refrigerated overnight covered with Optical Adhesive Film to prevent evaporation. The cDNA was added the next day. The plates were resealed with Optical Adhesive Film, and briefly spun to bring all contents to the bottoms of the wells. For RT-qPCR a QuantStudio 7 Flex (Catalog number 4485701, Applied Biosystems, Thermo Fisher Scientific, Waltham, MA 02451, United States) was used, set for 96 well plates, 0.1 ml

fast well, standard curve, and Fam, programmed with the following cycle times and temperatures: hold for 2 min at 50 °C, polymerase activation for 2 min at 95 °C, and PCR (40 cycles) denature at 95 °C for 1 second then anneal/extend at 60 °C for 20 seconds. The QuantStudio 7 Flex used QuantStudio real-time PCR software for calculations of the cycle threshold (Ct) and normalized reporter value (Rn). Results were exported to Excel files. Calculations were performed based on comparative Ct, to glyceraldehyde-3-phosphate dehydrogenase (GAPDH), means.

Eight cDNA replicates were prepared of each treatment condition (M0, M1-, and M2-like cells exposed to 0, 1, 10, or 100 µg/ml nanoceria). Duplicate samples were included in qPCR reactions of each. Probes were included for GAPDH (the housekeeping gene), Nos2 (nitric oxide synthase, a M1 cell marker), Ccr7 (chemokine (C-C motif) receptor 7, a M1 cell marker), Arg1 (arginase 1 gene, a M2 cell marker), and Mrc1 (mannose receptor, C type 1, a M2 cell marker).

Cell mito stress test (MST) and the glycolysis stress test (GST)

This was conducted on a Seahorse XFe96 Analyzer (Agilent, Santa Clara, CA 95051, United States). Standard Seahorse XF Cell MST or GST protocols were performed. Non-polarized (M0), M1-, and M2-like cells (8×10^3 cells/well) were grown in multiple wells in Seahorse XFe96 cell culture plates for ~ 44 h before MST or GST assays. For MST, oxygen consumption rates (OCR) were measured after stepwise injection of oligomycin (2.5 µM), carbonyl cyanide 4-(trifluoromethoxy)phenylhydrazone (FCCP) (4 µM), and rotenone (1 µM) and antimycin A (10 µM) that generated multiple states of cellular respiration. Glycolytic function (GST) was measured as extracellular acidification rate (ECAR) after stepwise injection of glucose (10 mM), oligomycin (4 µM), and 2-deoxyglucose (50 mM) that generated multiple states of glycolytic function. The mitochondrial and glycolytic function

parameters were generated using standard Seahorse data export for each MST and GST assay. At the end of the assay the protein concentration for each well was quantified using the BSA method and the rates were normalized to the protein concentration.

Immunocytochemistry

For immunocytochemistry, autoclaved coverslips were placed in PBS rinsed 35 mm dishes. RAW cells were added in 10% FBS, high glucose DMEM at 0.75, 1, and 0.5 x 10^4/dish, for M0 and M1- and M2-like subsequent polarization, respectively. Eighteen h later the cells were washed with 10% FBS phosphate-free DMEM. Nanoceria (0, 1, 10, or 100 µg/ml) were added. Nanoceria uptake and incubation took place for 2.5 h in a 37 ˚C, 5% CO_2 incubator. The cells were then washed once with normal saline solution, washed in 10% FBS-DMEM (plus phosphate), and polarized. The cells were then prepared for immunocytochemistry following a modified BioLegend protocol (2018 version) https://www.biolegend.com/en-us/protocols/immunocytochemistry-staining-protocol, as follows.

Donkey serum, antibodies, 4′,6-diamidino-2-phenylindole (DAPI), and phalloidin-AF488 solutions were sterilized through 0.22 µm filters. Cells were washed twice in PBS, then fixed in 4% *p*-formaldehyde-PBS (prepared from a 16% p-formaldehyde stock solution, 10x PBS, and sterile Milli-Q water) for 15 min, then five min washed three times in PBS. Cells were permeabilized in 0.5% Triton-X 100 for five min, followed by three five min PBS washes. Cells were separately treated with CD197 (CCR7) monoclonal Ab (4B12), APC for M1-like cell morphometry or goat α-mouse MMR/CD206, polyclonal for M2-like cell morphometry. Primary antibodies, 180 µl, were carefully placed onto the coverslip, and another coverslip was placed on top, creating an antibody sandwich. Dishes containing the coverslips were placed in a box with a tight-fitting lid with wet paper towels lining the bottom (humidified box) and incubated for ≥ 16 h at 4 ˚C. The top coverslip was floated off with PBS and discarded.

Cells were then washed with 0.1% Tween 20-PBS twice followed by PBS once, five min each. The secondary antibody (donkey α-goat-Alexa Fluor 594 (A11058)) was added in the same manner as the primary antibody for one h at room temperature. The top coverslip was floated off with PBS, and the cells washed with 0.1% Tween 20-PBS three times followed by PBS once, five min each. DAPI (1/4800 of 1 mg/ml stock) and phalloidin-AF488 (1/1000) in PBS were then added for 45 to 50 min at room temperature, followed by washing with 0.1% Tween 20-PBS four times then PBS once. The cells on the coverslips were mounted on slides using Vectashield held in place with nail polish. The slides were stored at -20 ˚C until confocal microscopy images were obtained.

To enable concurrent staining of the same cells for both CD197 (CCR7) and MMR/CD206, secondary antibodies were selected for their fluorescent emission that did not significantly overlap with each other, DAPI, or phalloidin. The procedures were the same with the following changes. Blocking buffer, 2% donkey serum in PBS, was added for one h, then aspirated. The antibodies were mixed in blocking buffer together; rat α-mouse CD197 at 1/200 and goat α-mouse CD206 at 1/100. The secondary antibodies (donkey α-rat-AF647 plus donkey α-goat-AF594 1/500 each) were added in the same manner as the above and incubated at 4 ˚C overnight.

Imaging

Imaging of treated and fluorescently-labeled cells was performed on a TCS SP8 confocal microscope (Leica Microsystems, Buffalo Grove, IL 60089 United States). Using the Navigator function in LAS-X, multiple z-stack frames were imaged for each slide with 16 bit depth. Conventional photomultipliers were used for APC, AF594, and AF647 fluors, while hybrid detectors were used for DAPI and AF488. Sequential scanning was used to minimize

cross-talk. Within each experiment, identical capture settings were used for all slides (laser power, pinhole, detector gain, offset, detection wavelengths).

Image Processing

Leica image files were imported into arivis Vision4D v3.5 (arivis AG, 18057 Rostock Germany). Z stacks for each frame of cells were analyzed using a pipeline to automatically detect cell boundaries. The segmentation pipeline was initiated with the detection of nuclei, based on DAPI staining. The consistency and low background for DAPI detection provided reliable identification of each cell in a field. To expand the area to each cell perimeter, two region-growing steps were employed. The first used the detection of anti-CD206 staining to define general cytoplasmic regions of each cell. Beginning from each defined nucleus, the selected segment was expanded to include the contiguous anti-CD206 signal. Although staining intensity for anti-CD206 varied with treatment, there was always sufficient signal above background to generally define cytoplasm. The final region growing step was to expand the segments defined by DAPI and anti-CD206 to also include contiguous phalloidin staining. The addition of the actin cytoskeleton provided sharp and distinct boundaries for each segment. See Figure 1 for single channel images and steps in the segmentation pipeline. The segments defined by the automated detection pipeline fit very well with the cell boundaries that were observed by eye, even for cells with extensive regions of contact with neighbors. After visual inspection of all images, manual curation was necessary for ~ 0.2% of the segments to remove, merge, or split segments, mostly due to duplicated nuclei in dividing cells or particularly long projections on some differentiated cells.

For each of the identified and verified segments in each field and for each treatment, morphometric and intensity measurements were recorded. From among the 16

measurements, the sum of the intensity for the M1 marker (CD197), the sum of the intensity for the M2 marker (CD206), cell volume, and roundness are presented here.

Polarization verification and nanoceria's effects on non- and polarized RAW cells

The methods in Supplementary Material, above, and following were utilized to verify polarization of RAW cells to M1- and M2-like phenotypes and assess nanoceria's effects on cell polarity.

A. To determine the IL-1β level, 2 x 10^6 cells were seeded in T-75 tissue culture flasks. RAW cells were polarized and then exposed to vehicle or 10 µg/ml nanoceria for six h. IL-1β was determined by a western blotting assay [45].

B. An arginase assay was conducted [46]. To assess the effects of nanoceria, cells were seeded at 1 x 10^5/well of 24-well plates and exposed to vehicle or 10 µg/ml nanoceria for 2.5 h the next day. The cells were then polarized. It was assumed that nanoceria would be taken up and retained by the cells, as reported in articles cited in the Introduction, and not washed out.

C. Expression of genes that are markers of M1- and M2-like cells (Nos2 and Ccr7) and (Arg1 and Mrc1), respectively, were determined in non-polarized (M0), and M1- and M2-like polarized RAW cells exposed to 0, 1, 10, or 100 µg/ml nanoceria as described above (Macrophage gene expression determined by RT-qPCR).

D. MST and GST assays were conducted as described above. After seeding and growth overnight in standard medium, the medium was replaced with the phosphate-free medium containing 0 (vehicle), 1, 10, or 100 µg/ml nanoceria for 2.5 h. Medium was then replaced with standard medium for 24 h containing PBS, LPS, or IL-4 to polarize the cells. Before starting the OCR and ECAR assays, the medium was replaced with Seahorse XF assay medium (pH 7.4) and the cells were acclimated for 1 h at 37 °C in a non-CO_2 incubator.

E. After polarization RAW cells were vehicle or nanoceria (10 µg/ml) exposed for six or 24 h then harvested and prepared for light microscopy by toluidine blue staining. Examples are shown in Figure S1. Selected morphological features (area, perimeter, and circularity) of the cells and their nuclei were manually traced and quantified using ImageJ version IJ 1.46r.

F. To assess nanoceria's effects on RAW cell polarization determined by immunohistochemistry, five experiments were conducted. The first experiment utilized separate (M0, M1-, and M2-like) cells stained for the M1- or M2-phenotype marker, and exposure to 0 or 10 µg/ml nanoceria. The second experiment utilized antibodies for the M1 and M2 phenotypes mixed together so that all three cell phenotypes received the same staining procedures. Cells were exposed to 0 or 10 µg/ml nanoceria. The last three experiments utilized the mixed antibodies for the M1 and M2 phenotypes. Cells were exposed to 0, 1, 10, or 100 µg/ml nanoceria.

Data and statistical analysis:

Results of the Il-1β assay were analyzed by a one-way ANOVA test, followed by a Dunnett's multiple comparisons test and an unpaired t-test. Results of the arginase assay was analyzed by a one-way ANOVA followed by a Tukey's multiple comparisons test. Cell OCR and GST results were analyzed by two-way ANOVAs, followed, when significant, by Tukey's multiple comparisons tests. Values of the morphological features of RAW cells after polarization were converted to log values and statistically significant differences compared to non-polarized (M0) cells determined by paired two-tailed t-tests or Wilcoxon tests. Mean results of the M1- and M2-like cells of the three immunohistochemistry experiments, as a percentage of M0 cells, for the M1 and M2 antibodies, volume, and roundness, were analyzed by one-way ANOVAs followed by a Tukey's multiple comparisons tests. GraphPad Prism 9.1.0 was used for these analyses. Values of the morphological features of RAW cells after polarization from each experiment were

converted to natural log and analyzed by a three-way ANOVA for polarity, treatment, and time, followed, when significant, by pair-wise comparisons. These analyses were done using JMP, version 15.2 from SAS, Inc. Results are presented as mean ± S.D.

Results

Polarization verification and nanoceria effects on non- and polarized RAW cells.

1. *IL-1β assay*

   The IL-1β level from M1-like cells was lower than M0 cells, presumably due to a decreased level of metabolism (Figure 2 left side) combined with increased IL-1β release earlier after LPS exposure. Nanoceria blocked the LPS-induced decrease (Figure 2 right side).

2. *Arginase assay*

   Interleukin 4 (IL-4) significantly increased arginase activity but LPS did not (Figure 3 left side). Nanoceria pretreatment significantly blocked the IL-4-induced arginase increase in M2-like RAW cells (Figure 3 right side).

3. *Macrophage gene expression determined by RT-qPCR*

   Expression of genes that characterize M1 (Nos2 and Ccr7) and M2 (Arg1 and Mrc1) macrophages were elevated in RAW cells following their polarization (Figure 4). Overall, the effects of nanoceria were to decrease gene expression of the polarization markers in all three cell phenotypes.

4. *Mito and glycolysis stress tests*

   Oxygen consumption rate determination showed LPS exposure produced almost complete mitochondrial shutdown (Figure 5). The M1-like cells had no measurable spare respiratory capacity (not shown). Nanoceria significantly increased several OCR and glycolytic M0 cell endpoints. It non-significantly increased all shown OCR endpoints in M1-like cells (Figure 5 A, B, and C) and its highest concentration significantly increased glycolytic capacity (Figure 5 E), reserve (Figure 5 F), and percent glycolytic reserve (Figure 5 G) in M1-like cells

toward M0 levels. It significantly decreased basal OCR (Figure 5 A), ATP production (Figure 5 C), and percent glycolytic reserve (Figure 5 G) in M2-like cells toward M0 levels.

5. *Macrophage morphology determined by light microscopy*

   Morphological features (area, perimeter, and circularity) determined from light microscopy images of the cells and their nuclei did not reveal a significant effect of time for all endpoints according to the three-way ANOVA for polarity, treatment, and time. Therefore, the six- and 24-h results were merged. Table 1 vehicle-exposed cells shows M1-like cells compared to M0 or M2-like cells exhibited greater nuclear and cell area and perimeter length and were less circular. Differences between M2-like and non-polarized (M0) cells were less pronounced.

   Comparison of selected morphometric properties of RAW cells after polarization followed by nanoceria exposure showed the same trend in differences between M1-like cells compared to M0 or M2-like cells as seen in the absence of nanoceria exposure (Table 1, compare Nanoceria-exposed cells to Vehicle-exposed cells). However, nanoceria exposure produced some significant changes (Table 1 Nanoceria compared to Vehicle-exposed cells).

6. *Macrophage morphology determined by immunohistochemistry*

   Examples of representative M0, M1-, and M2-like cells immunohistochemically stained, imaged using confocal microscopy, and defined using the arivis Vision4D pipeline that were not and were exposed to the three nanoceria concentrations are shown in Figure 6. The steps in segmentation and construction of a cell's volumetric rendering using the arivis Vision4D pipeline are shown in Figure 1 and in a movie in the Supplementary Material.

   Results of the five individual experiments utilizing immunohistochemical staining with DAPI, M1 and M2 cell antibodies, and phalloidin to determine M1 and M2 cell surface protein expression and cell volume and roundness of non-polarized RAW cells and cells polarized

to M1- and M2-like phenotypes are shown in the Supplemental Information (Figures and tables S2). Table 2 shows the combined results in the three cell phenotypes of all five experiments. Figure 7 shows the combined results in the M1- and M2-like cells of the three experiments that included the three nanoceria concentrations as a percentage of the non-nanoceria treated M0 cells of their same experiments.

Discussion

Multiple methods were utilized to address the hypothesis that nanoceria can increase inflammation/oxidative stress from the basal state and reduce it from the elevated state. Experiments were included to validate that LPS and IL-4, used by many others (cited in the Supplementary Material), polarized RAW cells to their M1 and M2 phenotypes, respectively. Lipopolysaccharide decreased the IL-1β level after six hour exposure (Figure 2); increased the expression of Nos2 and Ccr7 genes that characterize M1 macrophages (Figure 4); produced almost complete mitochondrial shutdown (Figure 5) as reported by others [47 48]; increased cell and nuclear size in light microscopic images (Table 1) as have been reported ([25 48 49 50]); increased cell volume (Table 2 and Figure 7); increased production of intracellular vacuoles and holes (Supplemental Information, Figure S1), as previously described [25]; and increased cell's M1 marker (CD197) intensity (Table 2 and Figure 7). Interleukin 4 increased arginase activity (Figure 3), a characteristic of M1 compared to non-polarized macrophages; the expression of Arg1 and Mrc1 genes that characterize M2 macrophages (Figure 4); oxidative metabolism (Figure 5) as reported by others [47]; and expression of the M1 cell surface protein (MMR/CD206) (Table 2 and Figure 7).

Multiple methods were also utilized to assess the effect of nanoceria exposure on the polarized RAW cells. Nanoceria blocked the LPS-induced IL-1β level decrease in M1-like cells, resulting in an IL-1β level comparable to M0 and M2-like cells (Figure 2). The two lower concentrations of

nanoceria decreased gene expression of the M1-like cell polarization markers toward M0 and M2-like cell levels (Figure 4). Nanoceria non-significantly increased OCR endpoints and its highest concentration significantly increased most glycolytic endpoints in M1-like cells toward M0 levels (Figure 5). Nanoceria reduced arginase expression to levels below those of M0 and M1-like cells (Figure 3) and concentration-dependently reduced gene expression of the M2-like cell polarization markers toward M0 and M1-like cell levels (Figure 4).

MST and GST results show a significant effect on mitochondrial and glycolytic function in response to LPS and IL-4 mediated M1 and M2 switch of the macrophages suggesting a shift in the metabolic function. Nanoceria distinctly affected mitochondrial and glycolytic parameters of M0, M1, and M2 macrophage phenotypes and in many cases in a dose dependent manner. In M0 macrophages, nanoceria increased basal respiration (Figure 5 A), maximal respiration (Figure 5 B), and ATP production (Figure 5 C) mainly at 1 and 10 µg/L nanoceria concentrations whereas the glycolytic capacity remained unaffected at those concentrations but was increased at 100 µg/L nanoceria (Figure 5 E). In M1 macrophages, with increasing nanoceria concentration there was a shift towards increasing basal respiration (Figure 5 A), maximal respiration (Figure 5 B), and ATP production (Figure 5 C). There was no change in basal glycolysis (Figure 5 D) but glycolytic capacity (Figure 5 E), glycolytic reserve (Figure 5 F), and percent reserve (Figure 5 G) were found to be significantly increased with nanoceria treatment in M1 macrophages. In M2 macrophages there was an increase in mitochondrial and glycolytic function parameters as compared to M0 macrophages. The nanoceria treatment in M2 macrophages resulted in decreased mitochondrial basal respiration (Figure 5 A), maximal respiration (Figure 5 B), and ATP synthesis (Figure 5 C) at 10 and 100 µg/L nanoceria. M2 cell glycolytic parameters were mostly unaffected with the nanoceria treatment. There were no significant differences in glycolytic parameters between the basal M0 glycolytic rate and nanoceria treated M2 macrophages. Overall, considering the multiple MST and GST metabolic

parameters, these results indicate a trend of the nanoceria treatment to bring the metabolic function towards the M0 macrophage states.

Light microscopic images of toluidine blue stained RAW cells were used to manually trace and quantify cell and nucleus area, perimeter, and circularity, to determine the effects of nanoceria on RAW cell polarization state. Nanoceria reduced M1-like cell nuclear and cell area and cell perimeter and increased circularity, bringing these endpoints closer to those of non-polarized (M0) cells (Table 1). Nanoceria also increased the area and perimeter of non-polarized (M0) cells, a change in the direction toward M1-like cell values. Nanoceria exposure induced changes in M2-like cell morphometry were not consistently changed toward M0 or M1-like cell values.

This study utilized a novel method to three-dimensionally characterize non-polarized and polarized macrophages. Polarized macrophage morphology has been described by many, but only two-dimensionally. M1 and M2 polarized murine-derived bone marrow-derived macrophages were described as round/oval, pancake-like shaped and having cellular elongation, respectively [27] [51]. Human primary macrophages polarized to the M1 phenotype had dendritic-like morphology with large filopodia whereas M2 macrophages were described as rounded with spindle-shaped morphology, similar to unstimulated macrophages [52]. Human monocyte M1-like cells were more elongated whereas M2-like cells had a larger, more rounded morphology [26]. Similarly, M2 macrophages from human monocytes had greater cell area than naive macrophages, that were larger than M1 macrophages, whereas the nuclear area for naive macrophages was greater than M1 or M2 phenotypes. M1 macrophages were more rounded whereas M2 macrophages had more irregular cell bodies [53]. M1 cells from human monocytes were described as spindle shaped and M2 cells as having a more spread morphology with giant multinucleated cells [54]. Non- and polarized canine blood-derived macrophages presented a different morphological picture [55]. M0 cells were small and round, averaging 8 µm diameter with

few cytoplasmic extensions, although ~ 25% had amoeboid morphology. Most M1 cells were amoeboid with an average diameter of 15 µm and had fibrillary processes extending from the cell surface. M2 cells exhibited a mixture of morphologies, including roundish and amoeboid shapes, and bipolar spindeloid cells up to 35 µm with elongated cell body with cytoplasmic extensions. Circularity was assessed using ImageJ, as conducted herein, to characterize macrophage phenotype [56]. It was also noted that M1-like cells exhibited a dendritic shape with cytoplasmic processes, compared to the round shape of non-polarized RAW cells [48 50], consistent with our findings. The greater size of M1-like RAW cells was quantified using a Coulter particle size analyzer [50]. The authors are not aware of reports of three-dimensional characterization of macrophage phenotypes.

Three-dimensional analysis of immunohistochemically-stained M0, M1- and M2-like RAW cells showed results consistent with similar endpoints of the two-dimensional analysis of stained cell cross-sections. M1-like cells had a greater volume than non-polarized cells (Table 2 and Figure 7), consistent with the greater area seen from the morphometric results obtained from the light microscopic images (Table 1). M1-like cells were less round than the non-polarized and M2-like cells (Table 2 and Figure 7), consistent with their lower two-dimensional circularity (Table 1). The three-dimensional analysis provided the added benefits of avoiding the time-consuming task of cell tracing for ImageJ analysis. It provided a three-dimensional representation of the entire cell from any viewpoint (Video).

Nanoceria exposure had no effect on non-polarized (M0) cell volume, had a tendency to increase their roundness (Table 2), and concentration-dependently decreased expression of the M1 and M2 proteins by the cells. Nanoceria exposure increased roundness of M1-like cells, consistent with the increased circularity of the light microscopic images, and concentration-dependently increased expression of the M2 protein of the M1-like cells (Table 2 and Figure 7),

changes away from the M1 phenotype. M2-like cell exposure to nanoceria showed greater volume (Table 2 and Figure 7), greater expression of the M1 marker protein, and less expression of the M2 marker protein, changes toward the M1 cell phenotype.

The results of the present studies are summarized in Table 3. Successful polarization of RAW cells to the M1-like phenotype is evidenced by greater expression of genes that characterize M1 macrophages; their larger nucleus area, cell size, and cell volume; and greater M1 antibody staining; than non-polarized (M0) cells. Successful polarization of RAW cells to the M2-like phenotype is evidenced by their higher arginase activity, greater expression of genes that characterize M1 macrophages, and less M1 and greater M2 antibody staining. Nanoceria produced effects on non-polarized RAW cells that suggested some polarization toward the M2 phenotype, including multiple endpoints of cell oxygen consumption rate and the glycolysis stress test. In contrast, nanoceria decreased expression of two M2 phenotypic genes, Arg1 and MRC1. Changes in M1-like cells in response to nanoceria exposure were largely in the direction to non-polarized and M2 cells, including the blocked decrease in IL1β; decreased expression of two M1 phenotypic genes, Nos2 and Ccr7 (although expression of the two M2 phenotypic genes (Arg1 and MRC1) was also reduced); decreased ATP production, blocked decrease in glycolytic capacity and increased glycolytic reserve; cells that were more circular (2D) and round (3D); and greater M2 antibody staining. Some of the results of M2-like cell nanoceria exposure suggest decrease of the M2 phenotype, including blockade of the M2 marker arginase activity, increased Ccr7 (a M1 marker) and decreased Arg1 and MRC1 (M2 marker) gene expression; decreased oxygen consumption rate and glycolytic reserve, and greater M1 and less M2 antibody staining. Overall, the results are consistent with the hypothesis that nanoceria can increase inflammation/oxidative stress from the basal state and reduce it from the elevated state.

Ceria-containing NPs have been shown to affect polarization status in the same direction as we observed. Adding manganese ferrite and ceria to mesoporous silica nanoparticles decreased proteins and mRNA that are preferentially expressed by M1 and increased those expressed by M2 bone marrow-derived macrophages [57]. Nanoceria produced changes in human monocytes that are consistent with the T helper 2 cell profile [43]. Nanoceria decreased the LPS-induced increase of TNF-α, IL-6, IL-1β, and nitrite production and iNOS and COX-2 protein by RAW cells, suggesting reduction of M1 activity [58]. Murine microglia (BV-2 cells) took up nanoceria and changed expression of phenotypic markers from those characterizing M1 to the M2 phenotype [59]. Cerium dioxide hydroxyapatite powder decreased RAW cell Ccr7, CD11c, IL-6, and TNFα and increased CD206, CD163, IL-10, IL-1ra, and TGF-β1 expression, suggesting activation toward the M2 phenotype [44]. In contrast, nanoceria was not found to alter phenotypic markers from human $CD14^+$ cells in the absence or presence of LPS pre-exposure [60].

In summary, a method was developed to three-dimensionally characterize the morphology of cells from antibody-stained RAW cells and confocal microscopy obtained images. It was utilized, along with cell OCR and GST assays, RT-qPCR of genes characterizing M1 and M2 macrophage phenotypes, and light microscopy of stained cells to test the hypothesis that nanoceria has the ability to increase inflammation/oxidative stress from the basal state and reduce it from the elevated state. Overall, the results support the hypothesis. The results help understand the conflict between reports that nanoceria has potential pharmaceutical benefit in the treatment of many conditions that has an inflammatory/oxidative stress component and reports demonstrating nanoceria-induced increased inflammation/oxidative stress. The results suggest that although nanoceria may be beneficial in the presence of elevated inflammation/oxidative stress, it should be avoided under normal circumstances.

Acknowledgements

Much thanks goes to Jim Begley, Imaging Center Manager, who worked with us to optimize the confocal imaging conditions and captured the many images used in this study. We thank Arvonn Tully, applications specialist from arivis AG, for advice and guidance in development of the pipeline used for segmentation and morphometric analysis of macrophages. We also thank Jarrod W. Creameans and Shekinah Alfaro for conducting the arginase and IL-1β assays, respectively, Cynthia Mattingly for advice on antibody assays, and Yasir Alsiraj and Rupinder Kaur for advice on qRT-PCR and PCR instrumentation, respectively.

Author contributions

Robert Yokel: Conceptualization, Funding acquisition, Methodology, Project administration, Formal analysis, Writing - original draft, Review & editing. Marsha Ensor: Investigation, Data curation, Writing original draft. Hemendra Vekaria: Investigation, Formal analysis. Patrick Sullivan: Formal analysis. David Feola: Methodology, Formal analysis. Arnold Stromberg: Formal analysis. Michael Tseng: Investigation, Visualization. Douglas Harrison: Conceptualization, Methodology, Visualization. All authors approved the submitted manuscript.

References

1. Deshpande S, Patil S, Kuchibhatla SV, Seal S. Size dependency variation in lattice parameter and valency states in nanocrystalline cerium oxide. *Appl Phys Lett* 2005; **87**: 133113/1-/3, 10.1063/1.2061873.
2. Younis A, Chu D, Li S. Cerium oxide nanostructures and their applications. InTech, 2016, p. 53-68, 10.5772/65937.
3. Yokel RA, Hancock ML, Cherian B, Brooks AJ, Ensor ML, Vekaria HJ, et al. Simulated biological fluid exposure changes nanoceria's surface properties but not its biological response. *Eur J Pharm Biopharm* 2019; **144**: 252-65, 10.1016/j.ejpb.2019.09.023.
4. Singh S. Cerium oxide based nanozymes: Redox phenomenon at biointerfaces. *Biointerphases* 2016; **11**: 04B202/1-04B/12, 10.1116/1.4966535.
5. Thakur N, Manna P, Das J. Synthesis and biomedical applications of nanoceria, a redox active nanoparticle. *J Nanobiotechnol* 2019; **17**: 1-27, 10.1186/s12951-019-0516-9.
6. Benameur L, Auffan M, Cassien M, Liu W, Culcasi M, Rahmouni H, et al. DNA damage and oxidative stress induced by CeO_2 nanoparticles in human dermal fibroblasts: Evidence of a clastogenic effect as a mechanism of genotoxicity. *Nanotoxicology* 2015; **9**: 696-705, 10.3109/17435390.2014.968889.
7. Ma JY, Mercer RR, Barger M, Schwegler-Berry D, Scabilloni J, Ma JK, et al. Induction of pulmonary fibrosis by cerium oxide nanoparticles. *Toxicol Appl Pharmacol* 2012; **262**: 255-64, 10.1016/j.taap.2012.05.005.
8. Guo C, Robertson S, Webber RJM, Buckley A, Warren J, Hodgson A, et al. Pulmonary toxicity of inhaled nano-sized cerium oxide aerosols in Sprague-Dawley rats. *Nanotoxicology* 2019; **13**: 733-50, 10.1080/17435390.2018.1554751.
9. Nalabotu SK, Kolli MB, Triest WE, Ma JY, Manne ND, Katta A, et al. Intratracheal instillation of cerium oxide nanoparticles induces hepatic toxicity in male Sprague-Dawley rats. *Int J Nanomed* 2011; **6**: 2327-35, 10.2147/IJN.S25119.

10. Tseng MT, Fu, Q., Lorc GK, Fernandez-Botran R, Deng Z-B, Graham UM, et al. Persistent hepatic structural alterations following nanoceria vascular infusion in the rat. *Toxicol Pathol* 2014; **42**: 984-96, doi: 10.1177/0192623313505780
11. Adebayo OA, Akinloye O, Adaramoye OA. Cerium oxide nanoparticle elicits oxidative stress, endocrine imbalance and lowers sperm characteristics in testes of balb/c mice. *Andrologia* 2018; **50**: e12920, 10.1111/and.12920.
12. Strickland JD, Lefew WR, Crooks J, Hall D, Ortenzio JNR, Dreher K, et al. *In vitro* screening of metal oxide nanoparticles for effects on neural function using cortical networks on microelectrode arrays. *Nanotoxicology* 2016; **10**: 619-28, 10.3109/17435390.2015.1107142.
13. Minarchick VC, Stapleton PA, Fix NR, Leonard SS, Sabolsky EM, Nurkiewicz TR. Intravenous and gastric cerium dioxide nanoparticle exposure disrupts microvascular smooth muscle signaling. *Toxicol Sci* 2015; **144**: 77-89, 10.1093/toxsci/kfu256.
14. Nemmar A, Al-Salam S, Beegam S, Yuvaraju P, Ali BH. Aortic oxidative stress, inflammation and DNA damage following pulmonary exposure to cerium oxide nanoparticles in a rat model of vascular injury. *Biomolecules* 2019; **9**: 376, 10.3390/biom9080376.
15. OECD. List of manufactured nanomaterials and list of endpoints for phase one of the sponsorship programme for the testing of manufactured nanomaterials: Revision. In: Environment Directorate, Joint Meeting of the Chemicals Committee and the Working Party on Chemicals, Pesticides and Biotechnology, (ed.). Series on the safety of manufactured nanomaterials. ENV/JM/MONO(2010)46 ed.: Organisation for Economic Co-operation and Development, 2010.
16. Lord MS, Jung M, Teoh WY, Gunawan C, Vassie JA, Amal R, et al. Cellular uptake and reactive oxygen species modulation of cerium oxide nanoparticles in human monocyte cell line U937. *Biomaterials* 2012; **33**: 7915-24, 10.1016/j.biomaterials.2012.07.024.
17. Plascencia-Villa G, Starr CR, Armstrong LS, Ponce A, José-Yacamán M. Imaging interactions of metal oxide nanoparticles with macrophage cells by ultra-high resolution

scanning electron microscopy techniques. *Integr Biol* 2012; **4**: 1358-66, 10.1039/c2ib20172k.

18. Zhou X, Wang B, Jiang P, Chen Y, Mao Z, Gao C. Uptake of cerium oxide nanoparticles and its influence on functions of mouse leukemic monocyte macrophages. *J Nanopart Res* 2015; **17**: 1-15, 10.1007/s11051-014-2815-2.
19. Selvaraj V, Nepal N, Rogers S, Manne NDPK, Arvapalli R, Rice KM, et al. Inhibition of MAP kinase/NF-kB mediated signaling and attenuation of lipopolysaccharide induced severe sepsis by cerium oxide nanoparticles. *Biomaterials* 2015; **59**: 160-71, 10.1016/j.biomaterials.2015.04.025.
20. Hussain S, Kodavanti PP, Marshburn JD, Janoshazi A, Marinakos SM, George M, et al. Decreased uptake and enhanced mitochondrial protection underlie reduced toxicity of nanoceria in human monocyte-derived macrophages. *J Biomed Nanotechnol* 2016; **12**: 2139-50, 10.1166/jbn.2016.2320.
21. Graham UM, Yokel RA, Dozier AK, Drummy L, Mahalingam K, Tseng MT, et al. Analytical high-resolution electron microscopy reveals organ specific nanoceria bioprocessing. *Toxicol Pathol* 2018; **46**: 47-61, 10.1177/0192623317737254.
22. Berry JP, Zhang L, Galle P, Ansoborlo E, Hengé-Napoli MH, Donnadieu-Claraz M. Role of alveolar macrophage lysosomes in metal detoxification. *Microsc Res Tech* 1997; **36**: 313-23, 10.1002/(SICI)1097-0029(19970215)36:4<313::AID-JEMT9>3.0.CO;2-M.
23. Lee KY. M1 and M2 polarization of macrophages: a mini-review. *Med Biol Sci Eng* 2019; **2**: 1-5, 10.30579/mbse.2019.2.1.1.
24. Agrawal A, Manchester M. Differential uptake of chemically modified cowpea mosaic virus nanoparticles in macrophage subpopulations present in inflammatory and tumor microenvironments. *Biomacromolecules* 2012; **13**: 3320-6, 10.1021/bm3010885.

25. Herd HL, Bartlett KT, Gustafson JA, McGill LD, Ghandehari H. Macrophage silica nanoparticle response is phenotypically dependent. *Biomaterials* 2015; **53**: 574-82, 10.1016/j.biomaterials.2015.02.070.
26. MacParland SA, Tsoi KM, Ouyang B, Ma XZ, Manuel J, Fawaz A, et al. Phenotype determines nanoparticle uptake by human macrophages from liver and blood. *ACS Nano* 2017; **11**: 2428-43, 10.1021/acsnano.6b06245.
27. Qie Y, Yuan H, von Roemeling CA, Chen Y, Liu X, Shih KD, et al. Surface modification of nanoparticles enables selective evasion of phagocytic clearance by distinct macrophage phenotypes. *Sci Rep* 2016; **6**: 26269, 10.1038/srep26269.
28. Hoppstädter J, Seif M, Dembek A, Cavelius C, Huwer H, Kraegeloh A, et al. M2 polarization enhances silica nanoparticle uptake by macrophages. *Front Pharmacol* 2015; **6**: 1-12, 10.3389/fphar.2015.00055.
29. Binnemars-Postma KA, ten Hoopen HW, Storm G, Prakash J. Differential uptake of nanoparticles by human M1 and M2 polarized macrophages: protein corona as a critical determinant. *Nanomed (London)* 2016; **11**: 2889-902, 10.2217/nnm-2016-0233.
30. Meng J, Li X, Wang C, Guo H, Liu J, Xu H. Carbon nanotubes activate macrophages into a M1/M2 mixed status: Recruiting naïve macrophages and supporting angiogenesis. *ACS Appl. Mater. Interfaces* 2015; **7**: 3180-8, 10.1021/am507649n.
31. Linares J, Fernández AB, Feito MJ, Matesanz MC, Sánchez-Salcedo S, Arcos D, et al. Effects of nanocrystalline hydroxyapatites on macrophage polarization. *J Mater Chem B* 2016; **4**: 1951-9, 10.1039/C6TB00014B.
32. Armstead AL, Li B. In vitro inflammatory effects of hard metal (WC-Co) nanoparticle exposure. *Int J Nanomed* 2016; **11**: 6195-206, 10.2147/IJN.S121141.
33. Zanganeh S, Hutter G, Spitler R, Lenkov O, Mahmoudi M, Shaw A, et al. Iron oxide nanoparticles inhibit tumour growth by inducing pro-inflammatory macrophage polarization in tumour tissues. *Nature Nanotechnology* 2016; **11**: 986-94, 10.1038/nnano.2016.168.

34. Yen H-J, Hsu S-h, Tsai C-L. Cytotoxicity and immunological response of gold and silver nanoparticles of different sizes. *Small* 2009; **5**: 1553-61, 10.1002/smll.200900126.
35. Fuchs A-K, Syrovets T, Haas KA, Loos C, Musyanovych A, Mailänder V, et al. Carboxyl- and amino-functionalized polystyrene nanoparticles differentially affect the polarization profile of M1 and M2 macrophage subsets. *Biomaterials* 2016; **85**: 78-87, 10.1016/j.biomaterials.2016.01.064.
36. Laskar A, Eilertsen J, Li W, Yuan X-M. SPION primes THP1 derived M2 macrophages towards M1-like macrophages. *Biochem Biophys Res Commun* 2013; **441**: 737-42, 10.1016/j.bbrc.2013.10.115.
37. Figueiredo P, Lepland A, Scodeller P, Fontana F, Torrieri G, Tiboni M, et al. Peptide-guided resiquimod-loaded lignin nanoparticles convert tumor-associated macrophages from M2 to M1 phenotype for enhanced chemotherapy. *Acta Biomater* 2021; **133**: 231-43, 10.1016/j.actbio.2020.09.038.
38. Pal R, Chakraborty B, Nath A, Singh LM, Ali M, Rahman DS, et al. Noble metal nanoparticle-induced oxidative stress modulates tumor associated macrophages (TAMs) from an M2 to M1 phenotype: An *in vitro* approach. *Int Immunopharmacol* 2016; **38**: 332-41, 10.1016/j.intimp.2016.06.006.
39. Su L, Zhang W, Wu X, Zhang Y, Chen X, Liu G, et al. Glycocalyx-mimicking nanoparticles for stimulation and polarization of macrophages via specific interactions. *Small* 2015; **11**: 4191-200, 10.1002/smll.201403838.
40. Jain S, Tran T-H, Amiji M. Macrophage repolarization with targeted alginate nanoparticles containing IL-10 plasmid DNA for the treatment of experimental arthritis. *Biomaterials* 2015; **61**: 162-77, 10.1016/j.biomaterials.2015.05.028.
41. Tran T-H, Krishnan S, Amiji MM. MicroRNA-223 induced repolarization of peritoneal macrophages using CD44 targeting hyaluronic acid nanoparticles for anti-inflammatory effects. *PLoS One* 2016; **11**: e0152024/1-e/14, 10.1371/journal.pone.0152024.

42. Ma JY, Zhao H, Mercer RR, Barger M, Rao M, Meighan T, et al. Cerium oxide nanoparticle-induced pulmonary inflammation and alveolar macrophage functional change in rats. *Nanotoxicology* 2011; **5**: 312-25, 10.3109/17435390.2010.513835.
43. Schanen BC, Das S, Reilly CM, Warren WL, Self WT, Seal S, et al. Immunomodulation and T helper TH_1/TH_2 response polarization by CeO_2 and TiO_2 nanoparticles. *PLoS One* 2013; **8**: e62816, 10.1371/journal.pone.0062816.
44. Li K, Shen Q, Xie Y, You M, Huang L, Zheng X. Incorporation of cerium oxide into hydroxyapatite coating regulates osteogenic activity of mesenchymal stem cell and macrophage polarization. *J Biomater Appl* 2017; **31**: 1062-76, 10.1177/0885328216682362.
45. Yokel RA, Tseng MT, Butterfield DA, Hancock ML, Grulke EA, Unrine JM, et al. Nanoceria distribution and effects are mouse-strain dependent. *Nanotoxicology* 2020; **14**: 827-46, 10.1080/17435390.2020.1770887.
46. Corraliza IM, Campo ML, Soler G, Modolell M. Determination of arginase activity in macrophages: a micromethod. *J Immunol Methods* 1994; **174**: 231-5, 10.1016/0022-1759(94)90027-2.
47. Koo S-j, Chowdhury IH, Szczesny B, Wan X, Garg NJ. Macrophages promote oxidative metabolism to drive nitric oxide generation in response to *Trypanosoma cruzi*. *Infect Immun* 2016; **84**: 3527-41, 10.1128/IAI.00809-16.
48. Scrima R, Menga M, Pacelli C, Agriesti F, Cela O, Piccoli C, et al. Para-hydroxyphenylpyruvate inhibits the pro-inflammatory stimulation of macrophage preventing LPS-mediated nitro-oxidative unbalance and immunometabolic shift. *PLoS One* 2017; **12**: e0188683/1-e/23, 10.1371/journal.pone.0188683.
49. Biswas S, Adrian M, Evdokimov K, Schledzewski K, Weber J, Winkler M, et al. Counter-regulation of the ligand-receptor pair Leda-1/Pianp and Pilralpha during the LPS-mediated immune response of murine macrophages. *Biochem Biophys Res Commun* 2015; **464**: 1078-83, 10.1016/j.bbrc.2015.07.079.

50. Saxena RK, Vallyathan V, Lewis DM. Evidence for lipopolysaccharide-induced differentiation of RAW264.7 murine macrophage cell line into dendritic like cells. *J Biosci* 2003; **28**: 129-34, 10.1007/BF02970143.
51. McWhorter FY, Wang T, Nguyen P, Chung T, Liu WF. Modulation of macrophage phenotype by cell shape. *Proc Natl Acad Sci U S A* 2013; **110**: 17253-8, 10.1073/pnas.1308887110.
52. Ploeger DTA, Hosper NA, Schipper M, Koerts JA, de Rond S, Bank RA. Cell plasticity in wound healing: paracrine factors of M1/ M2 polarized macrophages influence the phenotypical state of dermal fibroblasts. *Cell Commun Signal* 2013; **11**: 29, 10.1186/1478-811X-11-29.
53. Rostam HM, Reynolds PM, Alexander MR, Gadegaard N, Ghaemmaghami AM. Image based Machine Learning for identification of macrophage subsets. *Sci Rep* 2017; **7**: 1-11, 10.1038/s41598-017-03780-z.
54. Bertani FR, Mozetic P, Fioramonti M, Iuliani M, Ribelli G, Pantano F, et al. Classification of M1/M2-polarized human macrophages by label-free hyperspectral reflectance confocal microscopy and multivariate analysis. *Sci Rep* 2017; **7**: 1-9, 10.1038/s41598-017-08121-8.
55. Heinrich F, Lehmbecker A, Raddatz BB, Kegler K, Tipold A, Stein VM, et al. Morphologic, phenotypic, and transcriptomic characterization of classically and alternatively activated canine blood-derived macrophages *in vitro*. *PLoS One* 2017; **12**: e0183572/1-e/33, 10.1371/journal.pone.0183572.
56. Venter C, Myburgh KH, Niesler CU. Co-culture of pro-inflammatory macrophages and myofibroblasts: Evaluating morphological phenotypes and screening the effects of signaling pathway inhibitors. *Physiol Rep* 2021; **9**: e14704, 10.14814/phy2.14704.
57. Kim J, Kim HY, Song SY, Go S-h, Sohn HS, Baik S, et al. Synergistic oxygen generation and reactive oxygen species scavenging by manganese ferrite/ceria co-decorated nanoparticles for rheumatoid arthritis treatment. *ACS Nano* 2019; **13**: 3206-17, 10.1021/acsnano.8b08785.

58. Selvaraj V, Manne NDPK, Arvapalli R, Rice KM, Nandyala G, Fankenhanel E, et al. Effect of cerium oxide nanoparticles on sepsis induced mortality and NF-κB signaling in cultured macrophages. *Nanomed (London)* 2015; **10**: 1275-88, 10.2217/nnm.14.205.
59. Zeng F, Wu Y, Li X, Ge X, Guo Q, Lou X, et al. Custom-made ceria nanoparticles show a neuroprotective effect by modulating phenotypic polarization of the microglia. *Angew Chem Int Ed* 2018; **57**: 5808-12, 10.1002/anie.201802309.
60. Hussain S, Al-Nsour F, Rice AB, Marshburn J, Ji Z, Zink JI, et al. Cerium dioxide nanoparticles do not modulate the lipopolysaccharide-induced inflammatory response in human monocytes. *Int J Nanomed* 2012; **7**: 1387-97, 10.2147/IJN.S29429.

Figure legends:

Figure 1. An example of the confocal image components used to create the whole cell 3-D segment. A. DAPI-stained nuclei of M0 RAW264.7 cells. B. CD206 staining for a M2 macrophage marker protein. C. CD197 staining for a M1 macrophage marker protein. D. Phalloidin staining of actin filaments. E. Overlay of DAPI and CD206 staining. F. Overlay of DAPI, CD206, and phalloidin staining. G. 3D surface of selected segmented macrophage displayed in cyan. Detected boundaries of additional segments/cells are transparent to show underlying staining. H. The CD197 staining (not used in segmentation) is merged with the other three markers. The scale bar is 10 microns.

Figure 2. IL-1β level from non-polarized cells (M0), M1-, and M2-like RAW cells (left side) and the effect of nanoceria pretreatment (right side). ** = Significantly different from M0 cells by one-way ANOVA ($F(2,18) = 8.19$, $p = 0.0030$) and Dunnett's multiple comparisons test ($p = 0.0017$). Nanoceria pretreatment results are not significantly different ($F(2,18) = 0.47$), nor were the results from the M1-like non- and nanoceria-pretreated cells ($p = 0.2182$). Results are from seven experiments.

Figure 3. Arginase activity of non-polarized (M0), M1-, and M2-like RAW cells (left side) and the effect of nanoceria pretreatment (right side). *** and **** = Significantly different from non-pretreated M2 cells ($p < 0.001$) and ($p < 0.0001$) by one-way ANOVA ($F(5,16) = 14.05$, $p = < 0.0001$) and Tukey's multiple comparisons test. Results are from four experiments.

Figure 4. Expression of genes that characterize M1 (Nos2 and Ccr7) and M2 (Arg1 and Mrc1) polarized macrophages of RAW cells after their polarization and nanoceria exposure compared to non-polarized (M0) control (vehicle exposed) cells. Solid histograms are polarized control

(vehicle exposed) cells. Check patterned histograms are nanoceria-exposed cells. Note the different Y axis scales.

Figure 5. Macrophage polarization and nanoceria effects on the mito stress test (MST) and glycolysis stress test (GST) parameters. A) The basal OCR, B) maximal OCR and C) ATP production rates were determined from the MST whereas the D) glycolysis, E) glycolytic capacity, F) glycolytic reserve and G) percent glycolytic reserve were obtained from the GST. Numbers in parentheses are the nanoceria concentrations in µg/ml. *, **,*** and **** = significantly different from M0 cells; $^{+}$, $^{++}$, $^{+++}$, and $^{++++}$ = significantly different from M1-like cells; and $^{\#}$, $^{\#\#}$, $^{\#\#\#}$, and $^{\#\#\#\#}$ = significantly different from the same phenotype without nanoceria treatment, at $p < 0.05$, 0.01, 0.001, and 0.0001, respectively. All results are from Tukey's multiple comparisons tests comparing column means (main column effect) following a two-way ANOVA from which the column factor was significant at $p < 0.0001$. Results are from five experiments, each containing three to four replicates of each treatment condition.

Figure 6. Confocal image examples of the three cell phenotypes and four treatments. Representative cells were selected as those most closely having the average sum of the M1 and M2 antibodies, cell volume, and roundness for that cell phenotype (M0, M1-like, or M2-like) and treatment (0, 1, 10, or 100 µg/ml nanoceria). The lower right panel for each cell phenotype and treatment shows the CD206 antibody stain, color coded yellow. The lower left panel shows the CD197 antibody stain as magenta. The upper right panel shows the merged antibody stains including DAPI (blue) and phalloidin (green). The selected segmented cell is represented with a randomly colored solid surface in the upper left panel for each condition. Other segmented cells are represented as transparent surfaces. All images are displayed at comparable intensities and the same scale. Scale bar is 10 microns.

Figure 7. Results of the three immunohistochemistry experiments that included all three nanoceria concentrations to determine antibody staining, volume, and roundness of M0, M1-, and M2-like cells and nanoceria's effects, as a percentage of M0 cells that did not receive nanoceria pretreatment. ANOVA results for the M1 and M2 antibodies, volume, and roundness were $F(7,16) = 5.212$, 0.1699, 2.719, and 4.527, with $p = 0.0030$, 0.9980, 0.0462, and 0.0059, respectively. * and ** = significant differences by Tukey's multiple comparisons tests at $p < 0.05$ and $p < 0.01$, respectively.

Figure 1

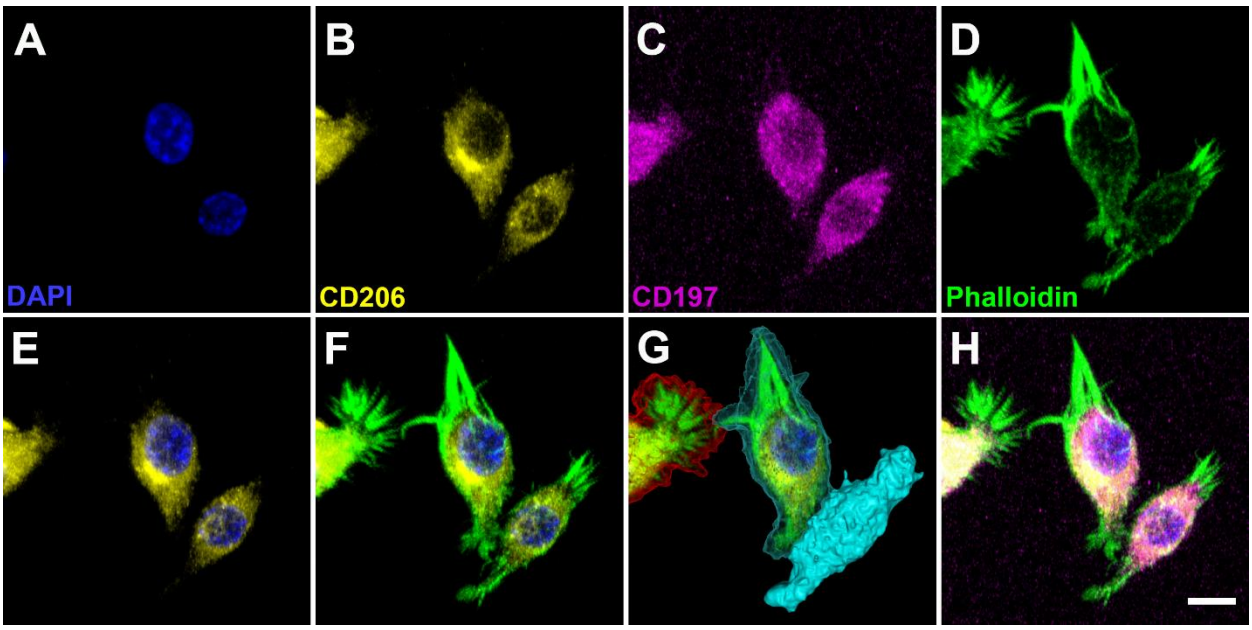

Figure 2

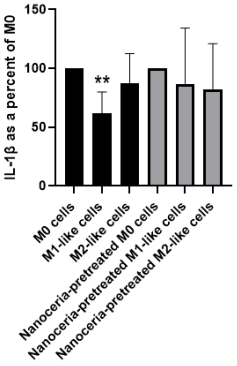
IL-1β as a percent of M0
150
100
50
0
**
M0 cells
M1-like cells
M2-like cells
Nanoceria-pretreated M0 cells
Nanoceria-pretreated M1-like cells
Nanoceria-pretreated M2-like cells

Figure 3

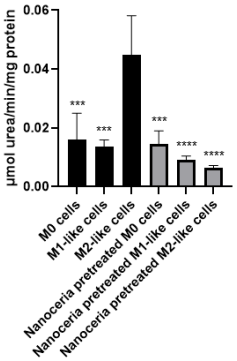
µmol urea/min/mg protein
0.06
0.04
0.02
0.00
***
***
***
****
****
M0 cells
M1-like cells
M2-like cells
Nanoceria pretreated M0 cells
Nanoceria pretreated M1-like cells
Nanoceria pretreated M2-like cells

Figure 4

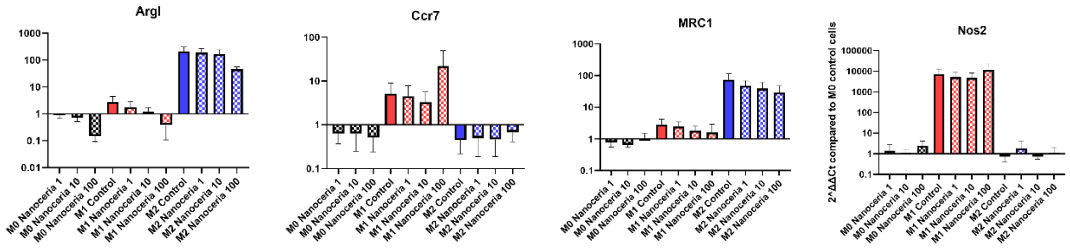
Arg1
Ccr7
MRC1
Nos2
2^-ΔΔCt compared to M0 control cells
M0 Nanoceria 1
M0 Nanoceria 10
M0 Nanoceria 100
M1 Control
M1 Nanoceria 1
M1 Nanoceria 10
M1 Nanoceria 100
M2 Control
M2 Nanoceria 1
M2 Nanoceria 10
M2 Nanoceria 100

Figure 5

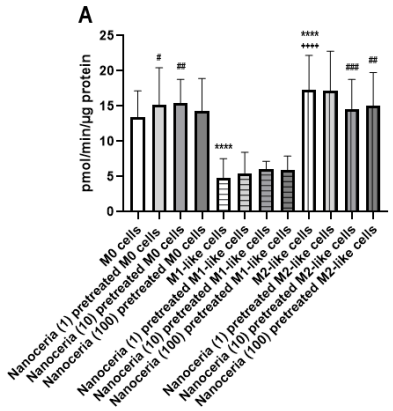
A
pmol/min/µg protein
25
20
15
10
5
0
#
##
****
****
****
###
##
M0 cells
Nanoceria (1) pretreated M0 cells
Nanoceria (10) pretreated M0 cells
Nanoceria (100) pretreated M0 cells
M1-like cells
Nanoceria (1) pretreated M1-like cells
Nanoceria (10) pretreated M1-like cells
Nanoceria (100) pretreated M1-like cells
M2-like cells
Nanoceria (1) pretreated M2-like cells
Nanoceria (10) pretreated M2-like cells
Nanoceria (100) pretreated M2-like cells

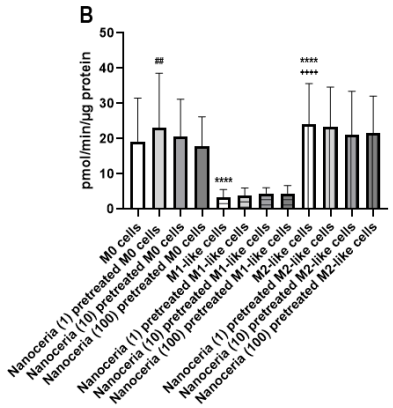
B
pmol/min/µg protein
50
40
30
20
10
0
##
****
****
M0 cells
Nanoceria (1) pretreated M0 cells
Nanoceria (10) pretreated M0 cells
Nanoceria (100) pretreated M0 cells
M1-like cells
Nanoceria (1) pretreated M1-like cells
Nanoceria (10) pretreated M1-like cells
Nanoceria (100) pretreated M1-like cells
M2-like cells
Nanoceria (1) pretreated M2-like cells
Nanoceria (10) pretreated M2-like cells
Nanoceria (100) pretreated M2-like cells

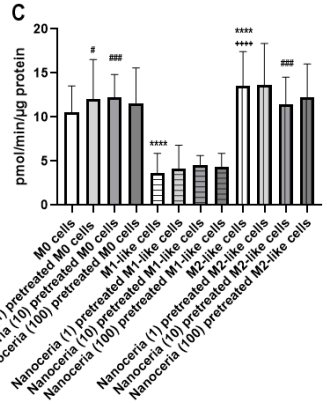
C
pmol/min/µg protein
20
15
10
5
0
#
###
****
****
****
###
M0 cells
Nanoceria (1) pretreated M0 cells
Nanoceria (10) pretreated M0 cells
Nanoceria (100) pretreated M0 cells
M1-like cells
Nanoceria (1) pretreated M1-like cells
Nanoceria (10) pretreated M1-like cells
Nanoceria (100) pretreated M1-like cells
M2-like cells
Nanoceria (1) pretreated M2-like cells
Nanoceria (10) pretreated M2-like cells
Nanoceria (100) pretreated M2-like cells

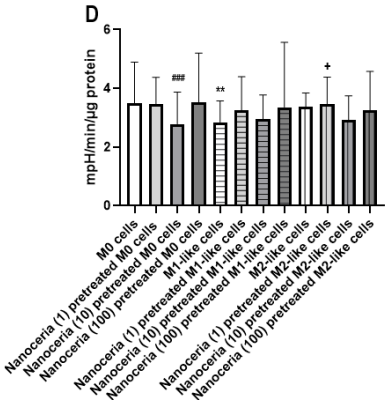
D
mpH/min/µg protein
6
4
2
0
###
**
+
M0 cells
Nanoceria (1) pretreated M0 cells
Nanoceria (10) pretreated M0 cells
Nanoceria (100) pretreated M0 cells
M1-like cells
Nanoceria (1) pretreated M1-like cells
Nanoceria (10) pretreated M1-like cells
Nanoceria (100) pretreated M1-like cells
M2-like cells
Nanoceria (1) pretreated M2-like cells
Nanoceria (10) pretreated M2-like cells
Nanoceria (100) pretreated M2-like cells

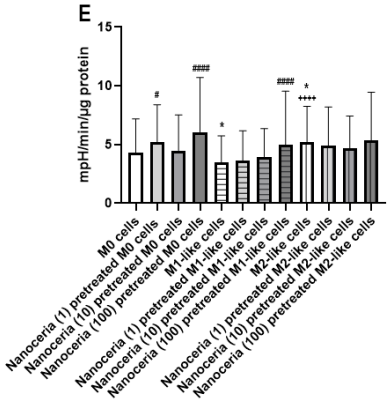
E
mpH/min/µg protein
15
10
5
0
#
####
*
####
*
++++
M0 cells
Nanoceria (1) pretreated M0 cells
Nanoceria (10) pretreated M0 cells
Nanoceria (100) pretreated M0 cells
M1-like cells
Nanoceria (1) pretreated M1-like cells
Nanoceria (10) pretreated M1-like cells
Nanoceria (100) pretreated M1-like cells
M2-like cells
Nanoceria (1) pretreated M2-like cells
Nanoceria (10) pretreated M2-like cells
Nanoceria (100) pretreated M2-like cells

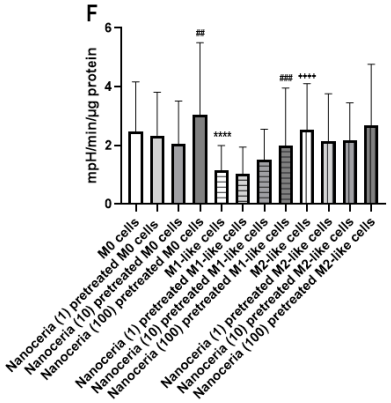
F
mpH/min/µg protein
6
4
2
0
##
****
###
++++
M0 cells
Nanoceria (1) pretreated M0 cells
Nanoceria (10) pretreated M0 cells
Nanoceria (100) pretreated M0 cells
M1-like cells
Nanoceria (1) pretreated M1-like cells
Nanoceria (10) pretreated M1-like cells
Nanoceria (100) pretreated M1-like cells
M2-like cells
Nanoceria (1) pretreated M2-like cells
Nanoceria (10) pretreated M2-like cells
Nanoceria (100) pretreated M2-like cells

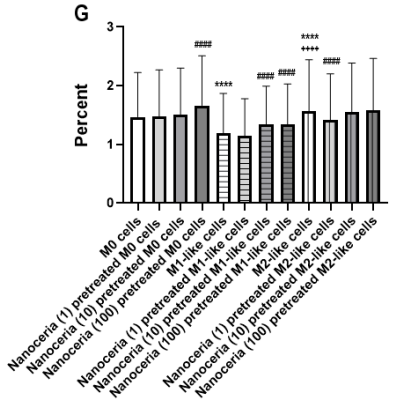
G
Percent
3
2
1
0
####
****
####
####
****
++++
####
M0 cells
Nanoceria (1) pretreated M0 cells
Nanoceria (10) pretreated M0 cells
Nanoceria (100) pretreated M0 cells
M1-like cells
Nanoceria (1) pretreated M1-like cells
Nanoceria (10) pretreated M1-like cells
Nanoceria (100) pretreated M1-like cells
M2-like cells
Nanoceria (1) pretreated M2-like cells
Nanoceria (10) pretreated M2-like cells
Nanoceria (100) pretreated M2-like cells

Figure 6

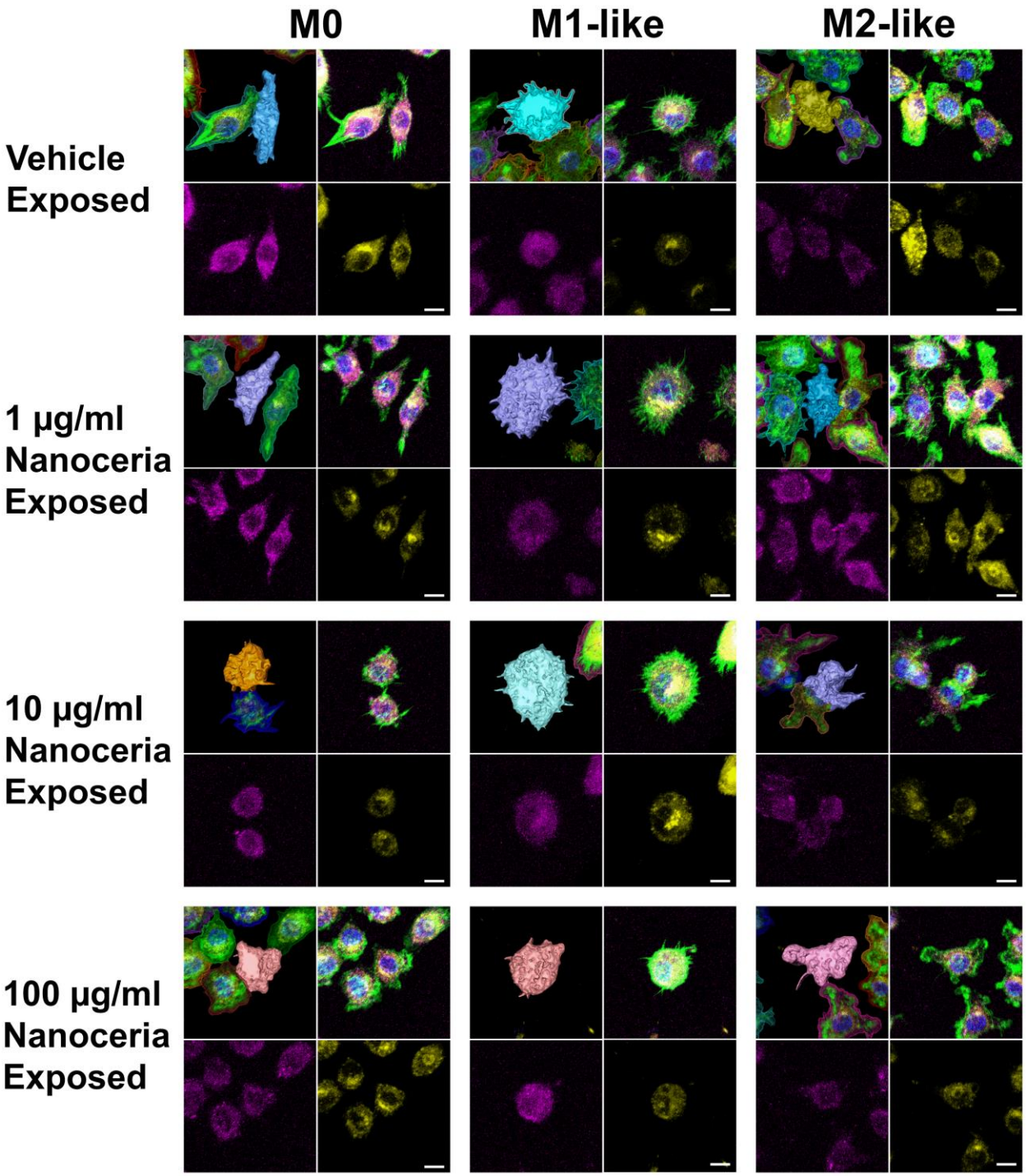
M0
M1-like
M2-like
Vehicle Exposed
1 µg/ml Nanoceria Exposed
10 µg/ml Nanoceria Exposed
100 µg/ml Nanoceria Exposed

Figure 7

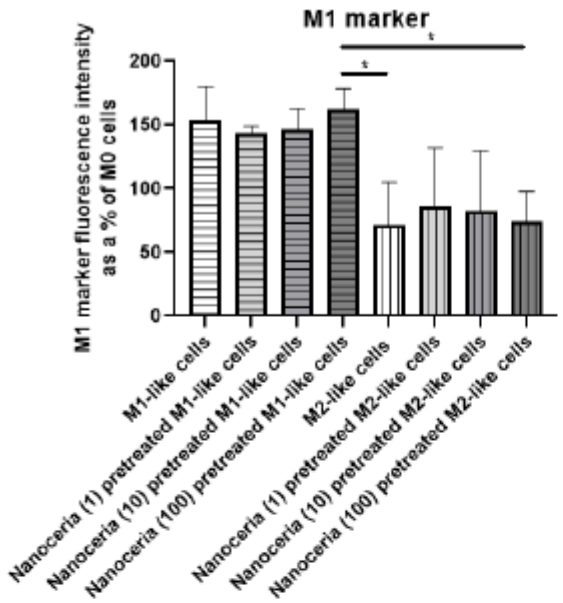
M1 marker
M1 marker fluorescence intensity as a % of M0 cells
200
150
100
50
0
*
*
M1-like cells
Nanoceria (1) pretreated M1-like cells
Nanoceria (10) pretreated M1-like cells
Nanoceria (100) pretreated M1-like cells
M2-like cells
Nanoceria (1) pretreated M2-like cells
Nanoceria (10) pretreated M2-like cells
Nanoceria (100) pretreated M2-like cells

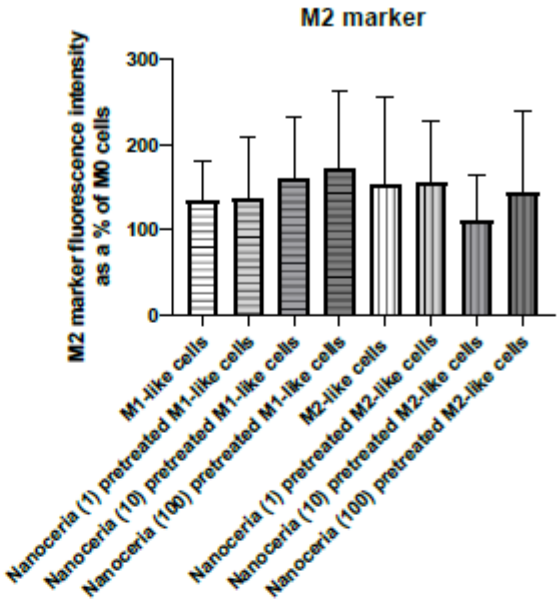
M2 marker
M2 marker fluorescence intensity as a % of M0 cells
300
200
100
0
M1-like cells
Nanoceria (1) pretreated M1-like cells
Nanoceria (10) pretreated M1-like cells
Nanoceria (100) pretreated M1-like cells
M2-like cells
Nanoceria (1) pretreated M2-like cells
Nanoceria (10) pretreated M2-like cells
Nanoceria (100) pretreated M2-like cells

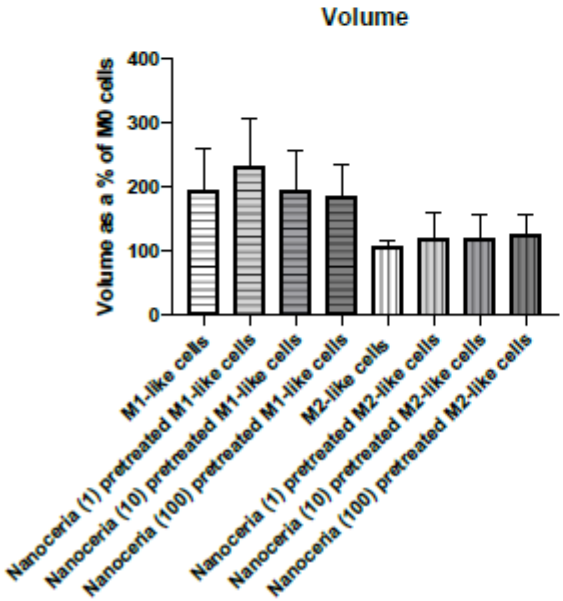
Volume
Volume as a % of M0 cells
400
300
200
100
0
M1-like cells
Nanoceria (1) pretreated M1-like cells
Nanoceria (10) pretreated M1-like cells
Nanoceria (100) pretreated M1-like cells
M2-like cells
Nanoceria (1) pretreated M2-like cells
Nanoceria (10) pretreated M2-like cells
Nanoceria (100) pretreated M2-like cells

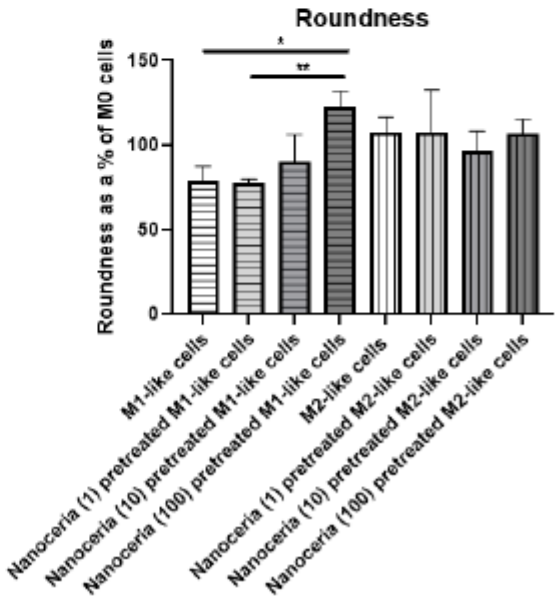
Roundness
Roundness as a % of M0 cells
150
100
50
0
*
**
M1-like cells
Nanoceria (1) pretreated M1-like cells
Nanoceria (10) pretreated M1-like cells
Nanoceria (100) pretreated M1-like cells
M2-like cells
Nanoceria (1) pretreated M2-like cells
Nanoceria (10) pretreated M2-like cells
Nanoceria (100) pretreated M2-like cells

Table 1. Nucleus and cell morphometric comparison of M0, M1-, and M2-like RAW cells after polarization and vehicle or nanoceria exposure. Values in parentheses are from pairwise comparisons following significant ANOVA results.

Light microscopy results						
	Nucleus			**Cell**		
	Area (μm²)	**Perimeter (μm)**	**Circularity**	**Area (μm²)**	**Perimeter (μm)**	**Circularity**
Vehicle-exposed cells						
M1-like compared to M0 cells	30.9/20.6 (****)	21.8/17.0 (****)	0.78/0.87 (****)	103/40.6 (****)	39.9/23.8 (****)	0.80/0.89 (***)
M1-like compared to M2-like cells	30.9/19.1 (****)	21.8/16.2 (****)	0.78/0.88 (****)	103/38.4 (****)	39.9/23.2 (****)	0.80/0.88 (**)
M2-like compared to M0 cells	19.1/20.6 (*)	16.2/17.0 (**)	0.88/0.87 (NS)	38.4/40.6 (**)	23.2/23.8 (NS)	0.88/0.89 (*)
Nanoceria-exposed cells						
M1-like compared to M0 cells	24.3/20.4 (****)	19.8/16.8 (****)	0.77/0.87 (***)	82.8/41.8 (****)	34.9/24.1 (****)	0.84/0.89 (*)
M1-like compared to M2-like cells	24.3/16.4 (****)	19.8/15.8 (****)	0.77/0.83 (**)	82.8/35.0 (****)	34.9/22.0 (****)	0.84/0.90 (**)
M2-like compared to M0 cells	16.4/20.4 (NS)	15.8/16.8 (NS)	0.83/0.87 (NS)	35.0/41.8 (****)	22.0/24.1 (****)	0.90/0.89 (NS)
Nanoceria compared to vehicle-exposed cells						
M0 cells	Smaller (NS)	Smaller (NS)	No change	Larger (*)	Larger (**)	No change
M1-like cells	Smaller (*)	Smaller (NS)	Less (NS)	Smaller (****)	Smaller (**)	More (*)
M2-like cells	Smaller (NS)	Smaller (*)	Less (**)	Smaller (NS)	Smaller (*)	More (NS)

NS, *, **, ***, **** = P > 0.05, < 0.05, < 0.01, < 0.001, < 0.0001, respectively

Vehicle-exposed cell nucleus results are based on 138, 71, and 137 M0, M1-, and M2-like cells, and cell results are based on 242, 44, and 170 M0, M1- and M2-like cells, respectively.

Nanoceria-exposed cell nucleus results are based on 75, 113, and 179 M0, M1-, and M2-like cells and cell results are based on 142, 92, and 83 M0, M1-, and M2-like cells, respectively.

Table 2. Results of the five immunohistochemistry experiments to determine antibody staining, volume, and roundness of M0, M1-, and M2-like cells and nanoceria's effects. Asterisks in parentheses show statistically significant differences from M0 (not nanoceria exposed) cells from the same experiments and in the square brackets the roundness ratio of M1-like cells after 100 µg/ml nanoceria vs no nanoceria, * and ** = P < 0.05 and < 0.01, respectively.

	M0 (vehicle or nanoceria exposed) cells	**M1 (vehicle or nanoceria exposed) cells**	**M2 (vehicle or nanoceria exposed) cells**
Sum of fluorescence intensity of the M1 marker (CD197) [1]			
Nanoceria exposure (µg/ml)			
0 (n = 3) [2]	3.93 ± 0.39		2.81 ± 1.47
0 (n = 5)	2.89 ± 1.46	4.89 ± 1.67 (**)	
1 (n = 3)	3.84 ± 1.37	5.65 ± 0.48 (**)	3.51 ± 2.06
10 (n = 5)	3.17 ± 0.74	5.50 ± 0.80 (*)	3.32 ± 2.11
100 (n = 3)	3.01 ± 0.92	6.41 ± 1.10 (*)	2.95 ± 1.06
Sum of fluorescence intensity of the M2 marker (CD206) [1]			
0 (n = 3)	2.92 ± 2.06	3.70 ± 2.07	
0 (n = 5)	2.37 ± 1.65		3.48 ± 1.63
1 (n = 3)	2.52 ± 1.26	3.75 ± 1.00	3.08 ± 1.52
10 (n = 5)	2.35 ± 0.91	3.77 ± 0.81	3.33 ± 1.38
100 (n = 3)	2.45 ± 0.85	4.14 ± 1.66	3.41 ± 1.68
Volume (µm^3)			
0 (n = 3)	6342 ± 916		
0 (n = 5)	5354 ± 1701	11769 ± 2796 (**)	6480 ± 676
1 (n = 3)	6896 ± 1722	14242 ± 2685	7418 ± 2488
10 (n = 5)	5372 ± 1546	12135 ± 1630 (**)	7122 ± 1074
100 (n = 3)	7674 ± 2183	11390 ± 1932	7900 ± 995
Roundness			
0 (n = 3)	0.247 ± 0.015		
0 (n = 5)	0.233 ± 0.044	0.171 ± 0.052	0.242 ± 0.061
1 (n = 3)	0.259 ± 0.014	0.191 ± 0.013 (**)	0.265 ± 0.047
10 (n = 5)	0.248 ± 0.049	0.193 ± 0.070	0.231 ± 0.047
100 (n = 3)	0.271 ± 0.018	0.302 ± 0.006 (*) [**]	0.264 ± 0.020

1 Antibody sum values are as entered x 10^8

2 Number of experiments

Table 3. A summary of this article's study results. Statistically significant results, as shown in the article, are noted by an asterisk (*).

Endpoint	Compared to non-polarized (M0) cells		Nanoceria effect		
	M1-like cells	M2-like cells	Non-polarized (M0) cells	M1-like cells	M2-like cells
IL1β assay					
IL1β	Lower *			Blocked decrease to a level not different from M0 cells *	
Arginase assay					
Arginase activity, a M2 macrophage marker		Higher *			Blocked increase to a level below M0 cell level *
Macrophage gene expression determined by RT-qPCR					
Nos2	Greater	Not different	Inconsistent increase	Decreased toward M0 and M2-like cell levels	No consistent change
Ccr7	Greater	Less	Decreased	Decreased toward M0 and M2-like cell levels	Increased toward M0 and M1-like cell levels
Arg1	Greater	Greater	Decreased	Decreased to M0 cell level	Decreased toward M0 and M1-like cell levels
MRC1	Greater	Greater	Decreased	Decreased toward M0 cell level	Decreased toward M0 and M1-like cell levels
Cell oxygen consumption rate and the glycolysis stress test					
Basal OCR	Lower *	Higher *	Increased * toward M2-like cells	Increased toward M0 cell level	Decreased * toward M0 cell level
Maximal respiration	Lower *	Higher *	Increased * toward M2-like cells	Increased toward M0 cell level	Decreased toward M0 cell level
ATP production	Lower *	Higher *	Increased * toward M2-like cells	Increased toward M0 cell level	Decreased * toward M0 cell level
Glycolysis	Lower *	Not different	Decreased * toward	Increased toward M0 cell level	

			M1-like cells		
Glycolytic capacity	Lower *	Higher *	Increased * to level similar to M2-like cells	Increased * to a level similar to M0 cells	
Glycolytic reserve	Lower *	Higher	Increased *	Increased * toward M0 cells	
Percent glycolytic reserve	Lower *	Higher *	Increased *	Increased * toward M0 cell level	Decreased * toward M0 cell level
Macrophage morphology determined by light microscopy					
Nucleus area	Larger *	Smaller *	Smaller	Reduced * toward M0 and M2-like cell levels	Reduced
Nucleus perimeter	Greater *	Smaller *		Reduced toward M0 and M2-like cell levels	Reduced *
Nucleus circularity	Less *				Less *
Cell area	Greater *	Smaller *	Increased * toward M1 cell level	Decreased * toward M0 and M2-like cell levels	Decreased
Cell perimeter	Greater *		Increased * toward M1 cell level	Decreased * toward M0 and M2-like cell levels	Decreased *
Cell circularity	Less *	Less *		Increased * toward M0 and M2-like cell levels	Increased
Macrophage morphology determined by immunohistochemistry					
M1 antibody staining	Greater *	Less	Decreased toward M2-like cell level	Increased	Increased toward M1-like cell level
M2 antibody staining	Greater	Greater	Decreased	Greater	Decreased toward M0 cell level
Cell volume	Greater *	Greater	No consistent change	No consistent change	Greater toward M1-like cell level
Roundness	Less	Not different	Increased *	Increased toward M0	No consistent change

				and M2-like cell levels *	